

Supporting Information

Accelerated terrestrial ecosystem carbon turnover and its drivers

Donghai Wu¹, Shilong Piao^{1,2,3*}, Dan Zhu⁴, Xuhui Wang¹, Philippe Ciais⁴, Ana Bastos⁵, Xiangtao Xu⁶, Wenfang Xu⁷

¹Sino-French Institute for Earth System Science, College of Urban and Environmental Sciences, Peking University, Beijing 100871, China.

²Key Laboratory of Alpine Ecology, Institute of Tibetan Plateau Research, Chinese Academy of Sciences, Beijing 100085, China.

³Chinese Academy of Sciences Center for Excellence in Tibetan Plateau Earth Science, Chinese Academy of Sciences, Beijing 100085, China.

⁴Laboratoire des Sciences du Climat et de l'Environnement (LSCE), CEA CNRS UVSQ, Gif Sur Yvette 91191, France.

⁵Department of Geography, Ludwig-Maximilians Universität, Luisenstr. 37, 80333, Munchen, Germany.

⁶Department of Ecology and Evolutionary Biology, Cornell University, Ithaca, NY 14853, USA.

⁷School of Atmospheric Sciences, Sun Yat-sen University, Zhuhai 519082, Guangdong, China.

Appendix S1 Clarification of τ_{eco} , r_{veg} , r_{soil} , τ_{veg} and τ_{soil}

It should be clarified that τ_{eco} represents the mean time that carbon atoms reside in the ecosystem from influx via NPP to outflux mainly via heterotrophic respiration and disturbance (e.g. fire). We further used r_{veg} and r_{soil} (including litter pools) to describe the mean residence time that carbon atoms reside in each system respectively at an ecosystem scale (Fig. S1a). In addition, if we treat the vegetation pools as a system for study, vegetation carbon turnover time (τ_{veg}) represents the mean time that carbon atoms reside in the vegetation system from influx via NPP to outflux mainly via litter fall and disturbance (e.g. fire) (Fig. S1b). Here, τ_{veg} equals to r_{veg} based on previous theory. However, if we treat the soil pools (including litter pools) as a system for study, soil carbon turnover time (τ_{soil}) represents the mean time that carbon atoms reside in the soil from influx via litter fall to outflux mainly via heterotrophic respiration and disturbance (e.g. fire) (Fig. S1c). Here, τ_{soil} may be longer than r_{soil} because all the carbon atoms from NPP are taken into account for r_{soil} while only carbon atoms from litterfall for τ_{soil} . Therefore, it is necessary to clarify the research system before learning the carbon turnover times to make sure of the targeted flowing carbon atoms. In this study, r_{veg} and r_{soil} are accurate terms for detailing the τ_{eco} .

Appendix S2 Model evaluation

Reliability of ecosystem models is important for exploring temporal changes of τ_{eco} . Therefore, in this section, we carefully evaluated the overall performance of ORCHIDEE-MICT based on the S3 simulation, the closest simulation to the real world, in four aspects: (1) ecosystem carbon storage, NPP and τ_{eco} on global scale; (2) ecosystem carbon storage, NPP and τ_{eco} on grid scale; (3) spatially climatic sensitivities of NPP and τ_{eco} ; and (4) temporal CO₂

exchanges between the atmosphere and the terrestrial biosphere. ORCHIDEE-MICT was also previously evaluated in more details than most other LSMs for the high latitudes for NPP and NPP-sensitivity to temperature, soil moisture, snow and water budgets, soil carbon and fires (Guimberteau et al., 2018). For the evaluation of static τ_{eco} , we choose the traditional method, ratio of carbon pool and carbon flux, as previous studies (Carvalhais et al., 2014) although the ecosystem is in non-steady state. In general, pool/flux based on observations provides a reference of the order of magnitude for τ_{eco} . Here, we select datasets used in previous researches for the 2000s in addition to specific high latitude datasets already used by Guimberteau et al. In total, four NPP datasets (Bloom, Exbrayat, van der Velde, Feng, & Williams, 2016; Jung et al., 2017; Kolby Smith et al., 2016; Zhao & Running, 2010), four datasets of vegetation carbon storage (Bloom et al., 2016; Carvalhais et al., 2014; Liu et al., 2015; Ruesch & Gibbs, 2008), two datasets of soil carbon storage (Carvalhais et al., 2014; Hugelius et al., 2013), and one litter carbon dataset (Bloom et al., 2016) were used. Uncertainties from the range between datasets were calculated for model evaluation.

First, for ecosystem carbon storage, NPP and τ_{eco} on global scale, we conducted the analysis for all ecosystem models from Trendy V6 (Le Quéré et al., 2018) (Fig. S3). Results indicate that only three models (CLM4.5 (3435 Pg C), ORCHIDEE-MICT (2982 Pg C), and VEGAS (2976 Pg C)) fall within the observed total ecosystem carbon storage (full soil depth, 3253 ± 354 Pg C), while others have significant underestimation. In contrast, NPP from most models are close or within the uncertainty bounds of observations (53 ± 5 Pg C yr^{-1}), which suggests that NPP related processes are relatively well represented in these models. NPP from ORCHIDEE-MICT (53 Pg C yr^{-1}) matches exactly the mean of the 4 datasets. For τ_{eco} , most

models underestimate the magnitude derived from observation-based datasets. Only τ_{eco} derived from ORCHIDEE-MICT (59 yr) falls in the uncertainty bounds from observation-based results (62 ± 8 yr).

Second, we only focus on the ORCHIDEE-MICT model for evaluating the static ecosystem carbon storage, NPP and τ_{eco} on grid scale (Fig. S4). For ecosystem carbon storage, ORCHIDEE-MICT generally captures the spatial patterns including the latitudinal gradients. In addition, it should be noticed that ORCHIDEE-MICT shows higher ecosystem carbon density than mean observations in high latitude, and that the uncertainties of different observation-based datasets in these regions are also noticeable. For NPP and τ_{eco} , patterns are also quite similar between ORCHIDEE-MICT and mean observations. However, in some arid and semi-arid regions (western China, sub-Saharan and central Australia), model and observation do not match. This phenomenon was also found for most of the ecosystem models (Carvalhais et al., 2014; Wu, Piao, Liu, Ciais, & Yao, 2018), mainly attributed to imperfect description of hydrological processes and water-carbon interactions in current models. Furthermore, in these regions, NPP variations are also large across different observation-based datasets, which increases uncertainties for evaluating τ_{eco} .

Third, we further investigated the global covariation of τ_{eco} with climate in terrestrial ecosystem, as in (Carvalhais et al., 2014; Thurner et al., 2016; Thurner et al., 2017). Here, following previous work (Wu et al., 2018), we estimated the local spatial sensitivity (multiple linear regression slope) of NPP and τ_{eco} to mean annual temperature (MAT) and mean annual precipitation (MAP) in $5^\circ \times 5^\circ$ moving windows around each 1° grid cell. For NPP (Fig. S5), spatial temperature and precipitation sensitivities from ORCHIDEE-MICT almost mirror to the

patterns from observations. In contrast, spatially climatic sensitivities of τ_{eco} from ORCHIDEE-MICT are comparable with the observation-based patterns (Fig. S6). However, it should be noticed that there is poor agreement between ORCHIDEE-MICT and observation in some arid and semi-arid regions, and this mismatch is mainly from the precipitation sensitivities of τ_{eco} (see underestimation of τ_{eco} in these water-limited regions highlighted above).

Fourth, to examine the reliability of ORCHIDEE-MICT on temporal scale, we evaluated the temporal CO₂ exchanges between the atmosphere and the terrestrial biosphere (Fig. S7). Here, we analyzed the CO₂ exchanges with individual ecosystem models and atmospheric inversions. Results suggest that CO₂ exchanges from ORCHIDEE-MICT results lie within the range of ecosystem models and atmospheric inversions. Even though we cannot evaluate the model for the whole time period since the industrial revolution, the high agreements also provide us confidence for learning the changes of τ_{eco} .

Overall, ORCHIDEE-MICT captures the static and dynamic patterns of carbon cycle well. Furthermore, the model evaluation also confirms the importance of discretizing the integral soil profile into multi-layers, and coupling the permafrost carbon cycling processes, which can largely enhance the performance of soil carbon module. Still, we should keep in mind that no model could reproduce the real world. ORCHIDEE-MICT also needs to reconsider the processes of carbon-water interactions in water-limited regions, and couple the nutrient cycling module, which is closely connected with carbon turnover processes. Furthermore, uncertainties from different observations also need to be noticed. Anyway, ORCHIDEE-MICT is an ideal ecosystem model for clarifying the temporal changes of carbon turnover at current stage.

Appendix S3 “Apparent change” phenomenon induced by pool/flux in non-steady state

“Apparent change” occurs when we compute the system carbon turnover times under non-steady state fluxes and pools. It will mislead our understanding in the background driving mechanisms for the changes of carbon turnover times. Next, we will elaborate the “apparent change” phenomenon with two cases using a prescribed carbon cycle model.

The simplified carbon cycle model includes three vegetation carbon pools (leaf, wood and root), one litter carbon pool, and three soil carbon pools (Fig. S8). NPP in this ecosystem is 1 kg C m⁻² yr⁻¹. Cycling rates of leaf, wood and root carbon are 1 yr⁻¹, 1/30 yr⁻¹ and 1 yr⁻¹. Cycling rates of litter carbon is 1/3 yr⁻¹. Cycling rates of active, slow and passive soil carbon are 1/5 yr⁻¹, 1/20 yr⁻¹ and 1/100 yr⁻¹. Carbon allocation fraction from NPP to leaf, wood and root are 0.3, 0.4 and 0.3. Transfer rates from leaf, wood, and root outflux to litter pool are 0.9, 0.9 and 1. Ten percentage of leaf and wood outflux is assumed to leave the ecosystem via external disturbance. Transfer rates from litter outflux to active pool and slow pool are 0.3 and 0.3. Transfer rates from active pool to slow pool and passive pool are 0.4 and 0.1. Transfer rates from slow pool to active pool and passive pool are 0.4 and 0.1. Transfer rates from passive pool to active pool are 0.5. Thus, the ecosystem can be described as a matrix form:

$$d\mathbf{X}(t)/dt = \dot{\mathbf{X}}(t) = \mathbf{A} \cdot \mathbf{X}(t) + \mathbf{B} \cdot \mathbf{U}(t) \quad (6)$$

Where $\dot{\mathbf{X}}(t) \in \mathbb{R}^{7 \times 1}$ is dynamics of carbon pools for year t . $\mathbf{A} \in \mathbb{R}^{7 \times 7}$ represents fixed cycling rates for each carbon pool and transfer rates between carbon pools. $\mathbf{X}(t) \in \mathbb{R}^{7 \times 1}$ is carbon storage for year t . $\mathbf{B} \in \mathbb{R}^{7 \times 1}$ describes the allocation proportions to pools. $\mathbf{U}(t) \in \mathbb{R}^{1 \times 1}$ is total influx from NPP for year t . Therefore, the matrixes can be written as:

$$\mathbf{A} = \begin{pmatrix} -1 & 0 & 0 & 0 & 0 & 0 & 0 \\ 0 & -0.033 & 0 & 0 & 0 & 0 & 0 \\ 0 & 0 & -1 & 0 & 0 & 0 & 0 \\ 0.9 & 0.03 & 1 & -0.333 & 0 & 0 & 0 \\ 0 & 0 & 0 & 0.1 & -0.2 & 0.02 & 0.005 \\ 0 & 0 & 0 & 0.1 & 0.08 & -0.05 & 0 \\ 0 & 0 & 0 & 0 & 0.02 & 0.005 & -0.01 \end{pmatrix},$$

$$\mathbf{B} = \begin{pmatrix} 0.3 \\ 0.4 \\ 0.3 \\ 0 \\ 0 \\ 0 \\ 0 \end{pmatrix}, -\mathbf{A}^{-1} \cdot \mathbf{B} = \begin{pmatrix} 0.3 \\ 12 \\ 0.3 \\ 2.79 \\ 2.63 \\ 9.78 \\ 10.15 \end{pmatrix} (\text{yr}), \mathbf{U} = 1 (\text{kg C m}^{-2} \text{ yr}^{-1})$$

When we simulated an initial steady state spin-up run ($\dot{\mathbf{X}}(t) = 0$), the carbon storage capacity can be expressed as:

$$\mathbf{X} = \begin{pmatrix} 0.3 \\ 12 \\ 0.3 \\ 2.79 \\ 2.63 \\ 9.78 \\ 10.15 \end{pmatrix} (\text{kg C m}^{-2}), \sum \mathbf{X} = 37.95 (\text{kg C m}^{-2}),$$

$$\tau(t) = \sum \mathbf{X}/\mathbf{U} = \sum (-\mathbf{A}^{-1} \cdot \mathbf{B}) = 37.95 \text{ yr}.$$

For the first case (Fig. S9a), we assumed that NPP has been increased by 1.5 times in 100 years (101-200 year) in responses to the CO₂ fertilization, and then stabilized after that time. Here, we fixed system parameters of \mathbf{A} (cycling rates and transfer rates) and \mathbf{B} (carbon allocation fraction). In this dynamic, non-steady ecosystem, vegetation and soil carbon storage has been increased because of enhanced carbon inputs, however, the increasing rates suggested a lag-effect in response to the enhanced NPP. In detail, stronger time-lag effects occurred with slower cycling rates for the carbon pools. Therefore, if we compute the ecosystem carbon turnover time using traditional pool/flux, it suggested a decreasing trend along with increasing

carbon flux. The phenomenon is called as “apparent change” because the intrinsic ecosystem carbon turnover time has not changed for all the time ($\sum(-\mathbf{A}(t)^{-1} \cdot \mathbf{B}(t)) = 37.95$ yr). Fig. S9a also shows that carbon turnover times via traditional pool/flux tend to unchanged value when the system approaches steady state along with constant influx.

For the second case (Fig. S9b), we assumed that deforestation has happened in the 101 year, and ecosystem has experienced catastrophic shifts from forest to cropland. In the processes, NPP decreased by two thirds, and the cycling rate of wood increased to 1 yr^{-1} . Here, we remained other parameters in \mathbf{A} and \mathbf{B} unchanged. In this dynamic, non-steady ecosystem, vegetation and soil carbon storage has been decreased because of reduced carbon inputs, however, the decreasing rates suggested a lag-effect in response to the reduced NPP. In detail, stronger time-lag effects occurred with slower cycling rates for the soil carbon pools. Therefore, if we compute the ecosystem carbon turnover times using traditional pool/flux, it suggests an increasing trend along with decreasing carbon flux. The phenomenon is also called as “apparent change” because the intrinsic ecosystem carbon turnover time has been shorten ($\sum(-\mathbf{A}(t)^{-1} \cdot \mathbf{B}(t)) = 26.35$ yr). Fig. S9b also shows that carbon turnover times via traditional pool/flux tend to 26.35 yr when the system approaches steady state along with constant influx.

In general, “apparent change” occurrence induced by lagged responses of ecosystem carbon pools with slower cycling rates (e.g. slow pool and passive pool) under the conditions of changes of carbon inputs caused by external environmental changes. The above cases clearly elucidated why it is incorrect to study the changes of ecosystem carbon turnover time with traditional pool/flux in a non-steady state system. The “apparent change” misled the changes of carbon turnover times and their driving mechanisms. Therefore, we recommend using the

matrix inversion method to study the changes of terrestrial ecosystem carbon turnover time and its drivers to avoid the potential false signals caused by “apparent change”.

Appendix S4 “Apparent change” phenomenon based on ORCHIDEE-MICT

Based on outputted variables from ORCHIDEE-MICT (Fig. S2), we tested the theory of dynamic carbon cycle in non-steady state. We computed the carbon turnover times with two method: (1) $\sum \mathbf{X}(t)/\mathbf{U}(t)$ from steady state assumption; and (2) $\sum(-\mathbf{A}(t)^{-1} \cdot \mathbf{B}(t))$ based on dynamic theory. The two values are similar if system is under steady state. In the results (Fig. S10), for 1860s, representing the early stage of the industrial revolution, the global ecosystem carbon turnover times both equal to 74 years using the two methods, suggesting steady state condition in this period. In contrast, for 2000s, representing current stage of development, the global ecosystem carbon turnover times are different, with 59 year using Ceco/NPP and 64 year using matrix inversion. The results suggested that 2000s is in non-steady state, and estimation of carbon turnover times with Ceco/NPP induced “apparent change” phenomenon with 8% underestimation for ORCHIDEE-MICT.

Furthermore, we also focused on the differences of τ_{eco} based on the two methods on grid scale in 2000s (Fig. S11). Results indicated that Ceco/NPP underestimates the actual τ_{eco} at high northern latitudes and in southern China, and overestimates τ_{eco} in some grassland regions and in India. This “apparent change” difference can be reasonably explained by the theory in Appendix S3. In boreal regions and China, global warming, CO₂ fertilization and afforestation enhance primary productivity while the ecosystem carbon pools with slower cycling rates usually show lagged responses. This mismatch of responses on time scale lead to underestimation of τ_{eco} . By contrast, transitions from forests to grassland and cropland by land

use change (Fig. S19) usually reduced regional primary productivities. Similarly, the ecosystem carbon pools with slower cycling rates response much slower, which could account for the overestimation of τ_{eco} .

Figure legends:

Figure S1. Schematic representation of the concepts of carbon turnover times. (a), ecosystem carbon turnover time (τ_{eco}), carbon residence time in vegetation (r_{veg}) and carbon residence time in soil (r_{soil}). τ_{eco} represents the mean time that carbon atoms reside in the ecosystem from influx via NPP to outflux mainly via heterotrophic respiration (HR) and disturbance (e.g. fire). (b), vegetation carbon turnover time (τ_{veg}), which represents the mean time that carbon atoms reside in the vegetation system from influx via NPP to outflux mainly via litterfall and disturbance (e.g. fire). (c), soil carbon turnover time (τ_{soil}), which represents the mean time that carbon atoms reside in the soil from influx via litter fall to outflux mainly via heterotrophic respiration and disturbance (e.g. fire). Here, τ_{veg} equals to r_{veg} , and τ_{soil} may be longer than r_{soil} because all the carbon atoms from NPP are taken into account for r_{soil} while only carbon atoms from litterfall for τ_{soil} . More details are described in appendix S1.

Figure S2. Basic structure of carbon cycle processes in ORCHIDEE-MICT model. In this new version, there are five vegetation pools (fruit, leaf, reserve, root and wood), four litter pools (aboveground metabolic (AM) and structural (AS) litter pools, and belowground metabolic (BM) and structural litter (BS) pools), and three soil pools (active, slow and passive) for each soil layer. More details of ORCHIDEE-MICT are described in the method part.

Figure S3. Ecosystem carbon storage (a), NPP (b) and τ_{eco} (c) in 2000s on global scale. Here, we conducted the analysis for all ecosystem models from Trendy V6. Ensemble of model represents the mean value (with $\pm 1\sigma$ uncertainty) of all ecosystem models; and ensemble of data represents the mean value (with $\pm 1\sigma$ uncertainty in shading) derived from independent

observation datasets. For ORCHIDEE-MICT, ecosystem carbon storage and τ_{eco} with 3m soil depth are also displayed as purple pentagrams. More details are described in appendix S2.

Figure S4. Ecosystem carbon storage (a, b), NPP (c, d) and τ_{eco} (e, f) in 2000s on grid scale. (a), (c), and (e) are derived from observations; (b), (d), and (f) are derived from ORCHIDEE-MICT. Ensemble of data represents the mean value derived from independent observation datasets. The insets are maps of the patterns of coefficient of variation across observation datasets. More details are described in appendix S2.

Figure S5. Spatial patterns of apparent climatic sensitivities of NPP in a $5^\circ \times 5^\circ$ moving window using multiple linear regressions. (a)-(b), temperature and precipitation sensitivities of NPP derived from observations; (c)-(d), temperature and precipitation sensitivities of NPP derived from ORCHIDEE-MICT. The insets are maps of the patterns of consistency of sign using independent observation datasets compared with the data-ensemble. More details are described in appendix S2.

Figure S6. Spatial patterns of apparent climatic sensitivities of τ_{eco} in a $5^\circ \times 5^\circ$ moving window using multiple linear regressions. (a)-(b), temperature and precipitation sensitivities of τ_{eco} derived from observations; (c)-(d), temperature and precipitation sensitivities of τ_{eco} derived from ORCHIDEE-MICT. The insets are maps of the patterns of consistency of sign using independent observation datasets compared with the data-ensemble. More details are described in appendix S2.

Figure S7. CO₂ exchanges between the atmosphere and the terrestrial biosphere with ecosystem models and atmospheric inversions. Here, the ecosystem models include all models from

Trendy V6; and the atmospheric inversions contain three independent models (CAMS, Jena CarboScope and CTE). Values from multi-model mean (with $\pm 1\sigma$ uncertainty in shading) and ORCHIDEE-MICT are depicted. See more details in Global Carbon Budget 2017 (Le Quéré et al., 2018). Results suggested that CO₂ exchanges from ORCHIDEE-MICT are highly agreed with the mean of ecosystem models and atmospheric inversions. More details are described in appendix S2.

Figure S8. Simplified ecosystem carbon cycle model for illustrating the ecosystem carbon turnover time (τ_{eco}) under dynamic system in non-steady state. The simplified carbon cycle model includes three vegetation carbon pools (leaf, wood and root), one litter carbon pool, and three soil carbon pools. NPP in this ecosystem is 1 kg C m⁻² yr⁻¹. The case model is used for elaborating the “apparent change” phenomenon in Appendix S3.

Figure S9. Illustration of the “apparent change” phenomenon induced by CO₂ fertilization and land use change. For the first case (a), we assumed that NPP has been increased by 1.5 times in 100 years (101-200 year) in responses to the CO₂ fertilization, and then stabilized after that time. For the second case (b), we assumed that deforestation has happened in the 101 year, and ecosystem has experienced catastrophic shifts from forest to cropland. In both cases, when estimating τ_{eco} with Ceco/NPP, “apparent change” occurred by lagged responses of ecosystem carbon pools with slower cycling rates (e.g. slow pool and passive pool) under the conditions of changes of carbon inputs caused by external environmental changes. See detailed illustration of “apparent change” in Appendix S3.

Figure S10. Global ecosystem carbon turnover times (τ_{eco}) in 1860s and 2000s based on

ORCHIDEE-MICT model simulations. Two methods, matrix inversion and Ceco/NPP, are used for calculating the τ_{eco} . For 1860s, representing the early stage of the industrial revolution, the global ecosystem carbon turnover times are both 74 year using the two method, suggesting a steady state system in this period. In contrast, for 2000s, representing current stage of development, the global ecosystem carbon turnover times are different, with 59 year using Ceco/NPP and 64 year using matrix inversion. The results suggest that 2000s is in non-steady state, and estimation of carbon turnover times with Ceco/NPP induces “apparent change” phenomenon with 8% underestimation for ORCHIDEE-MICT.

Figure S11. Ratio of estimated τ_{eco} based on the two methods (Ceco/NPP and $\Sigma(-\mathbf{A}(t)^{-1} \cdot \mathbf{B}(t))$) on grid scale in 2000s. Here, “apparent change” mainly occurred at high northern latitudes and in southern China with an underestimation, and in some grassland regions and in India with an overestimation. See detailed explanations of the “apparent change” phenomenon in Appendix S4.

Figure S12. Attribution of changes of ecosystem carbon turnover times (τ_{eco}) between 1860s and 2000s on biome scale. (a)-(c), changes of τ_{eco} , r_{veg} and r_{soil} in boreal forest (BOF). (d)-(f), changes of τ_{eco} , r_{veg} and r_{soil} in temperate forest (TEF). (g)-(i), changes of τ_{eco} , r_{veg} and r_{soil} in tropical forest (TRF). (j)-(l), changes of τ_{eco} , r_{veg} and r_{soil} in grassland (GRA). (m)-(o), changes of τ_{eco} , r_{veg} and r_{soil} in cropland (CRO). Here, driving factors include CO₂ increasing (CO₂), climate change (CLI) and land use change (LUC). Furthermore, τ_{eco} is divided into carbon residence time in vegetation (r_{veg}) and in soil (r_{soil} , including litter pools). Asterisk represents that there is significant difference ($p < 0.05$) between 1860s and 2000s for τ_{veg} , r_{veg} and r_{soil} .

under different sceneries.

Figure S13. Spatial patterns of ecosystem carbon turnover times (τ_{eco}) in 1860s and 2000s. (a)-(b), spatial patterns of τ_{eco} in 1860s and 2000s. (c)-(d), spatial patterns of r_{veg} in 1860s and 2000s. (e)-(f), spatial patterns of r_{soil} in 1860s and 2000s. Here, τ_{eco} equals to the summation of carbon residence time in vegetation (r_{veg}) and in soil (r_{soil} , including litter pools).

Figure S14. Attribution of changes of ecosystem carbon turnover times (τ_{eco}) between 1860s and 2000s on grid scale. Driving factors include CO₂ increasing (CO₂), climate change (CLI) and land use change (LUC). Furthermore, τ_{eco} is divided into carbon residence time in vegetation (r_{veg}) and in soil (r_{soil} , including litter pools). (a)-(c), influences by CO₂ increasing, climate change and land use change. (d)-(f), influences by CO₂ increasing and climate change. (g)-(i), influences by CO₂ increasing. (j)-(l), influences by climate change. (m)-(o), influences by land use change. Stippling indicates locations that there is significant difference ($p < 0.05$) between 1860s and 2000s for τ_{eco} , r_{veg} and r_{soil} under different sceneries.

Figure S15. Fire effects on τ_{eco} , r_{veg} and r_{soil} in 1860s and 2000s. The spatial patterns are derived from the relative differences of simulation with fire-on compared with simulation with fire-off.

Figure S16. Relative changes of τ_{eco} , r_{veg} and r_{soil} in 1860s and 2000s for simulations of fire-on and fire-off on global scale. It is suggested that there are no significant differences of the relative changes of τ_{eco} between the two simulations, indicating weak effects of fire on changes of τ_{eco} .

Figure S17. Relative changes of τ_{eco} , r_{veg} and r_{soil} in 1860s and 2000s for simulations of fire-on and fire-off on grid scale. It is suggested that there are no significant differences of the relative

changes of τ_{eco} between the two simulations, indicating weak effects of fire on changes of τ_{eco} .

Figure S18. Total ecosystem carbon storage (Ceco) change and potential in different continents between 1860s and 2000s (a). Furthermore, dynamics of vegetation carbon storage (Cveg) and soil carbon storage (Csoil, including litter carbon) are showed in (b) and (c).

Figure S19. Spatial patterns of biome fraction in 1860s and 2000s and their changes. (a)-(c), boreal forest (BOF). (d)-(f), temperate forest (TEF). (g)-(i), tropical forest (TRF). (j)-(l) grassland (GRA). (m)-(o), cropland (CRO).

Figure S20. Spatial patterns of major biome for each grid in 1860s and 2000s based on ORCHIDEE-MICT model. Biomes include boreal forest (BOF), temperate forest (TEF), tropical forest (TRF), grassland (GRA), cropland (CRO) and bare land (BAR). (a), land cover map in 1860s. (b), land cover map in 2000s.

Figure S21. Relationship between vegetation carbon residence time (r_{veg}) and wood carbon residence time (estimated by wood allocation rate (ALLw) and wood turnover rate (Kw)) in 1860s by grid values using ORCHIDEE-MICT model. Results indicate that mean wood carbon residence time accounts for 93% of r_{veg} . Therefore, ALLw and Kw are suggested as main drivers of r_{veg} .

Figure S22. Changes of physical variables and physiological variables between 1860s and 2000s based on different driving scenarios on global and biome scale. (a), global scale. (b), boreal forest (BOF). (c), temperate forest (TEF). (d), tropical forest (TRF). (e), grassland (GRA). (f), cropland (CRO). Five scenarios include influences by CO₂ increasing, climate change and

land use change; influences by CO₂ increasing and climate change; influences by CO₂ increasing; influences by climate change; and influences by land use change. Physical variables include air temperature (TAS), precipitation (PRE), soil temperature (ST), soil moisture (SM), evapotranspiration (ET), vegetation evaporation (Eveg), soil evaporation (Esoil), vegetation transpiration (T), and total runoff (mrro). Physiological variables include net primary production (NPP), wood allocation of NPP (ALLw), wood turnover rate (Kw), litter carbon storage (Clit), decomposition rate of litter (Klit), decomposition rate of active pool (Ka), decomposition rate of slow pool (Ks), decomposition rate of passive pool (Kp), transfer rate from litter pool to active pool (littoa), transfer rate from litter pool to slow pool (littos), transfer rate from active pool to slow pool (atos), transfer rate from active pool to passive pool (atop), transfer rate from slow pool to active pool (stoa), transfer rate from slow pool to passive pool (stop), and transfer rate from passive pool to active pool (ptoa). Physical variables are showed as absolute changes (2000s minus 1860s), and physiological variables are showed as relative changes (2000s compares to 1860s). Black asterisk represents that there is significant difference ($p < 0.05$) between 1860s and 2000s for respective variables or physiological variables.

Figure S1

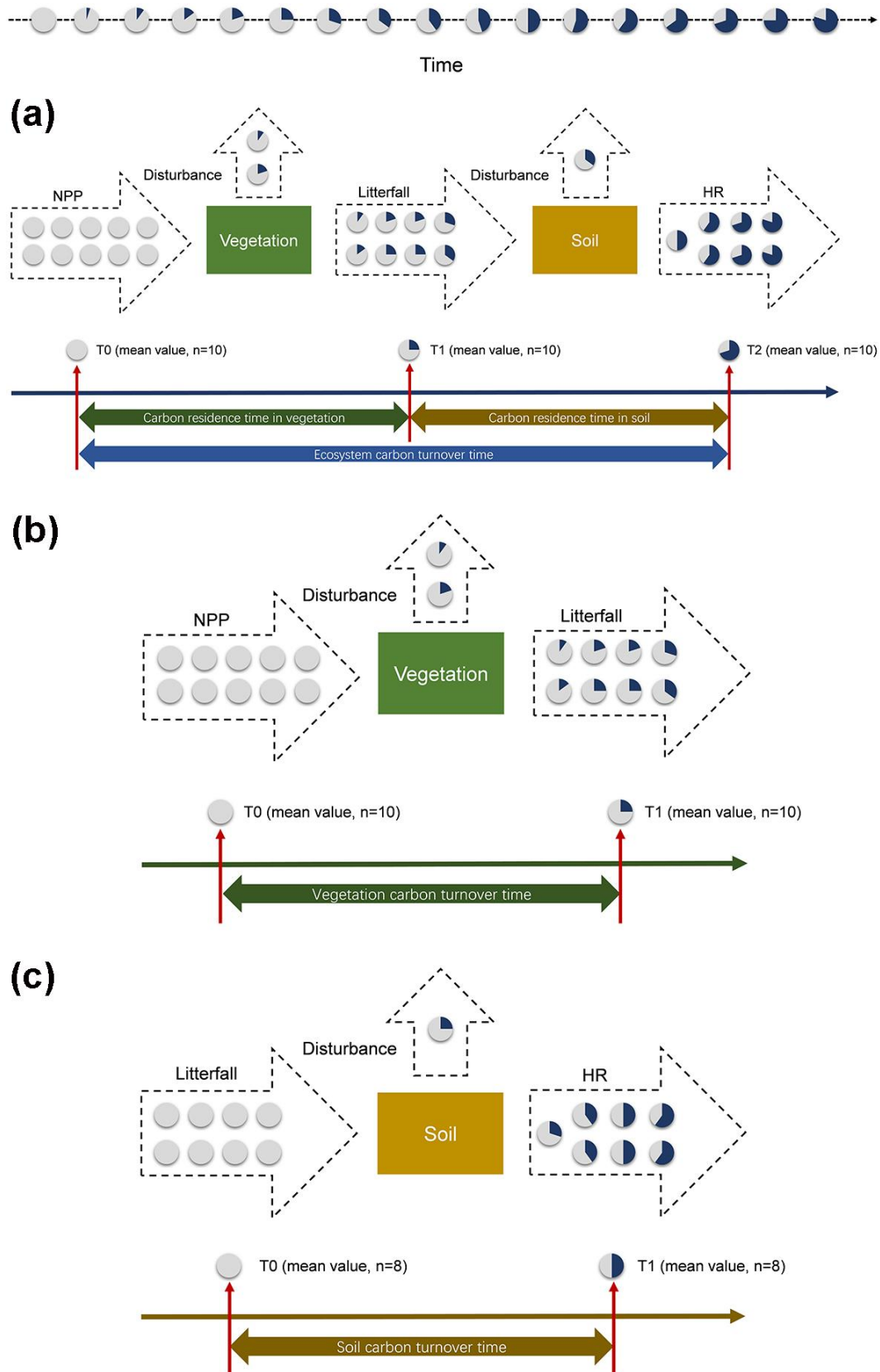


Figure S2

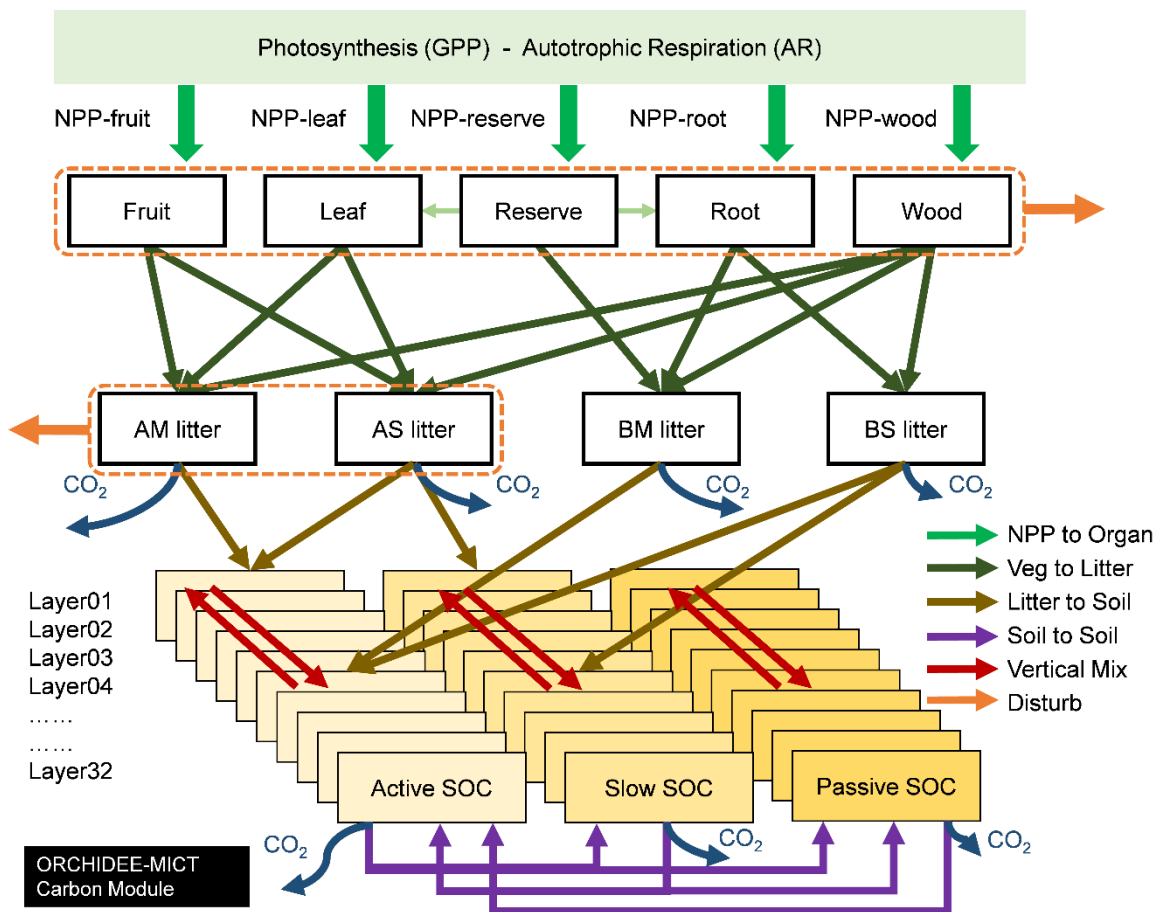


Figure S3

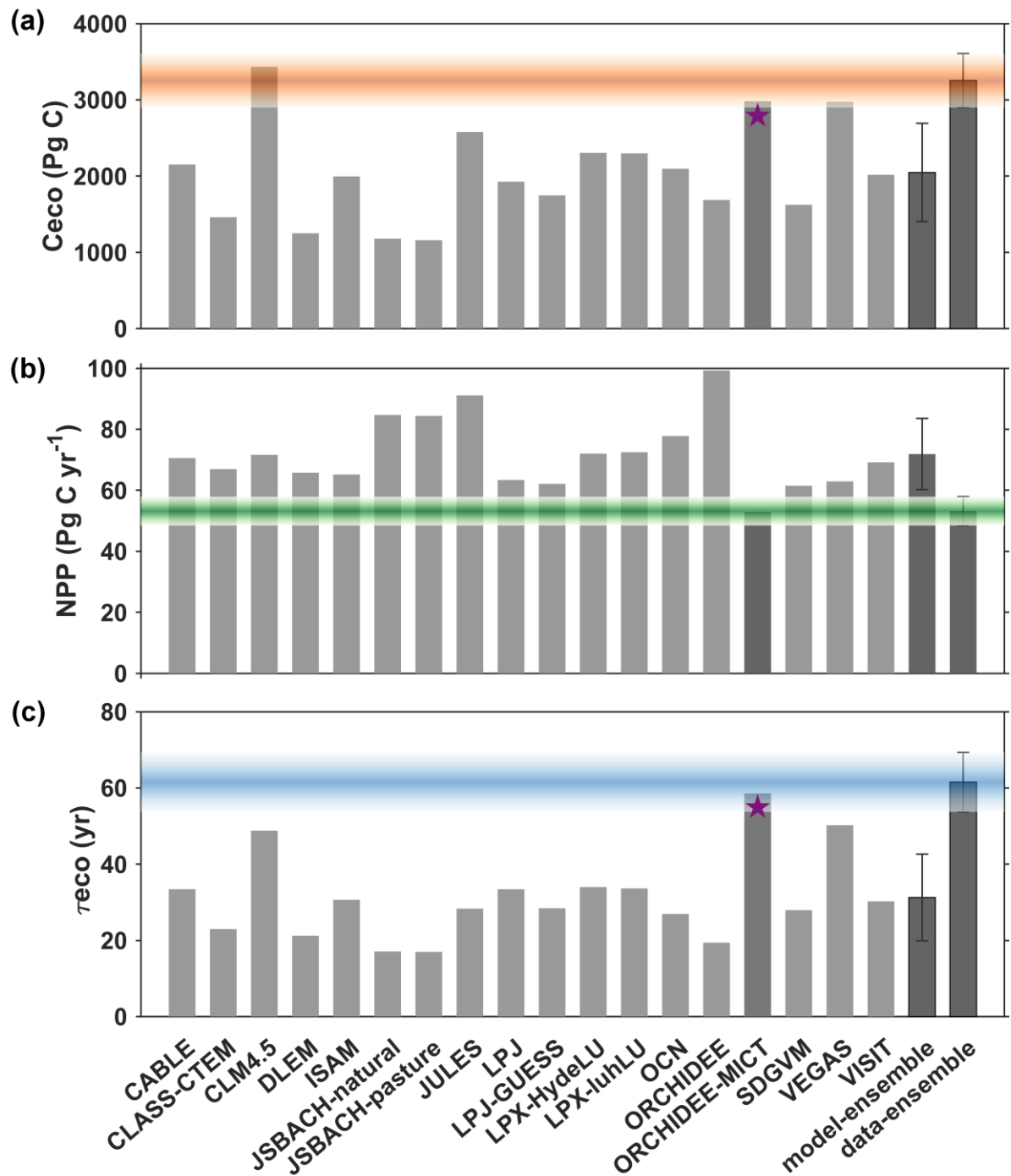


Figure S4

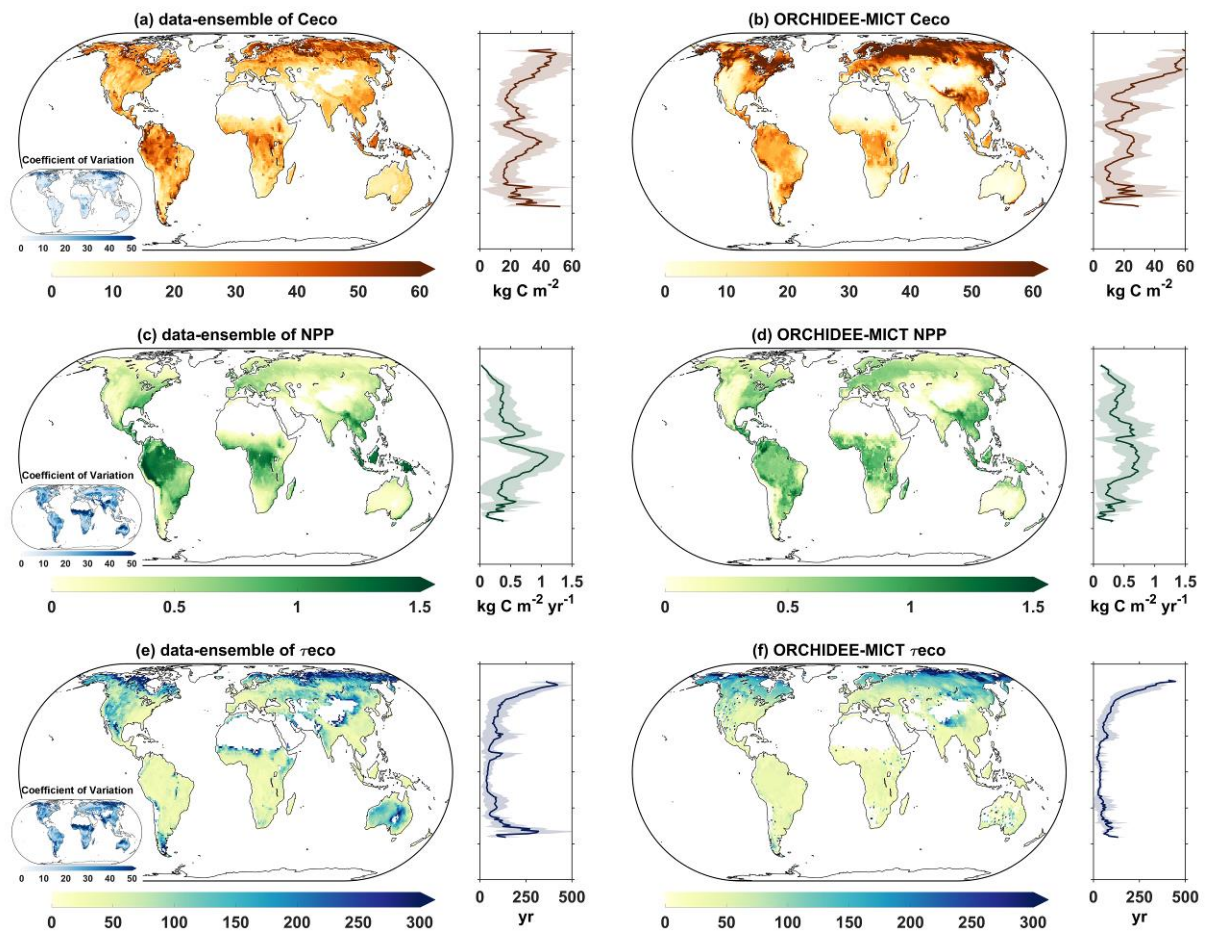


Figure S5

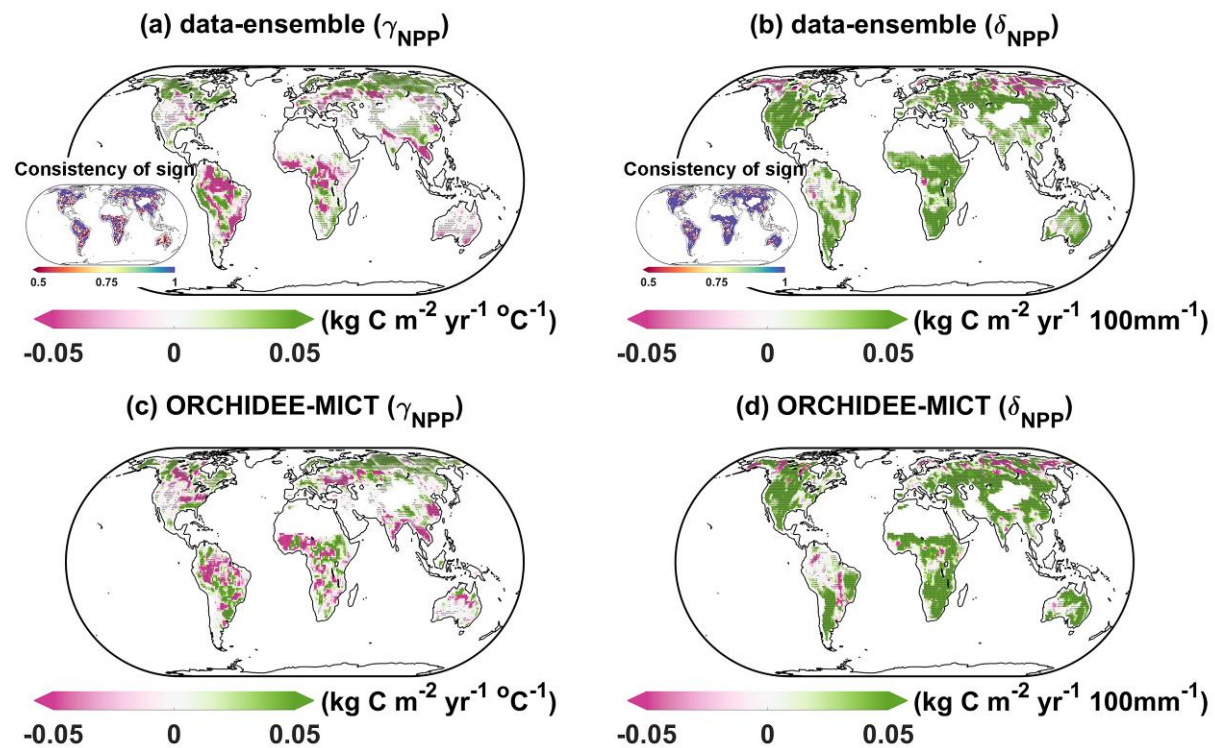


Figure S6

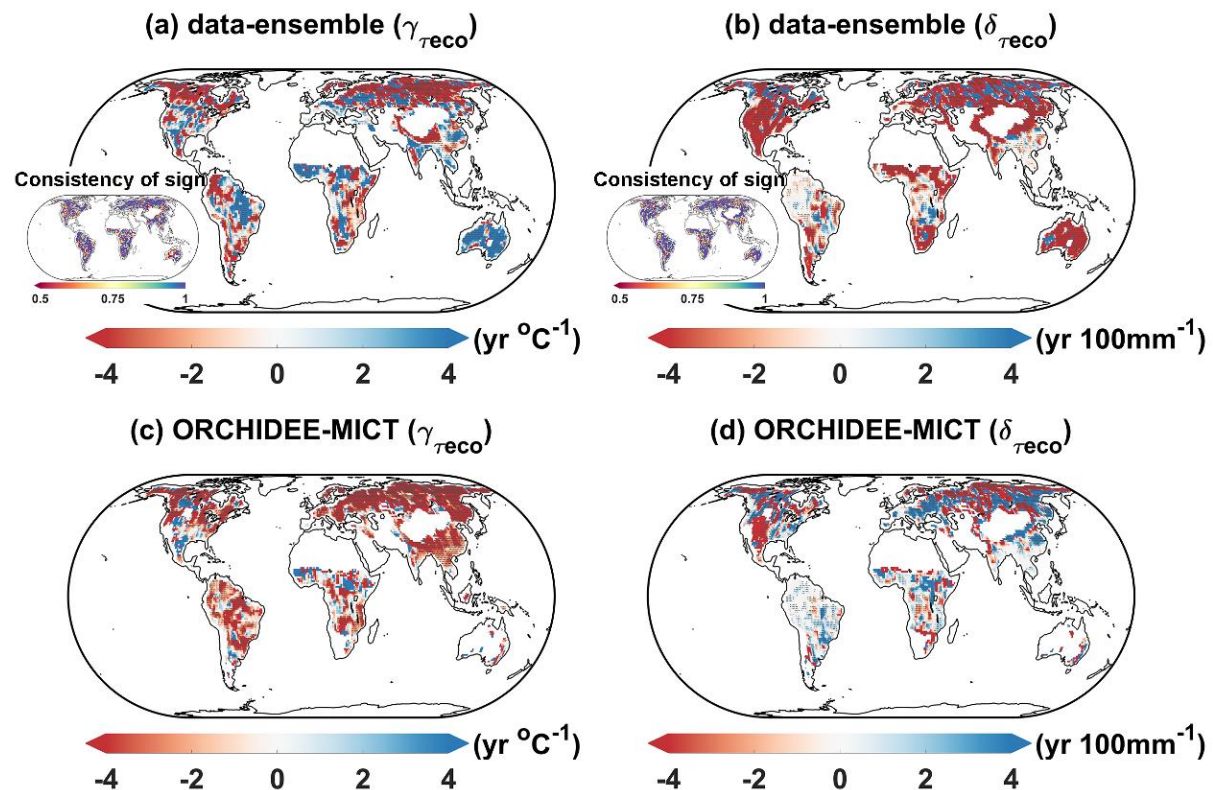


Figure S7

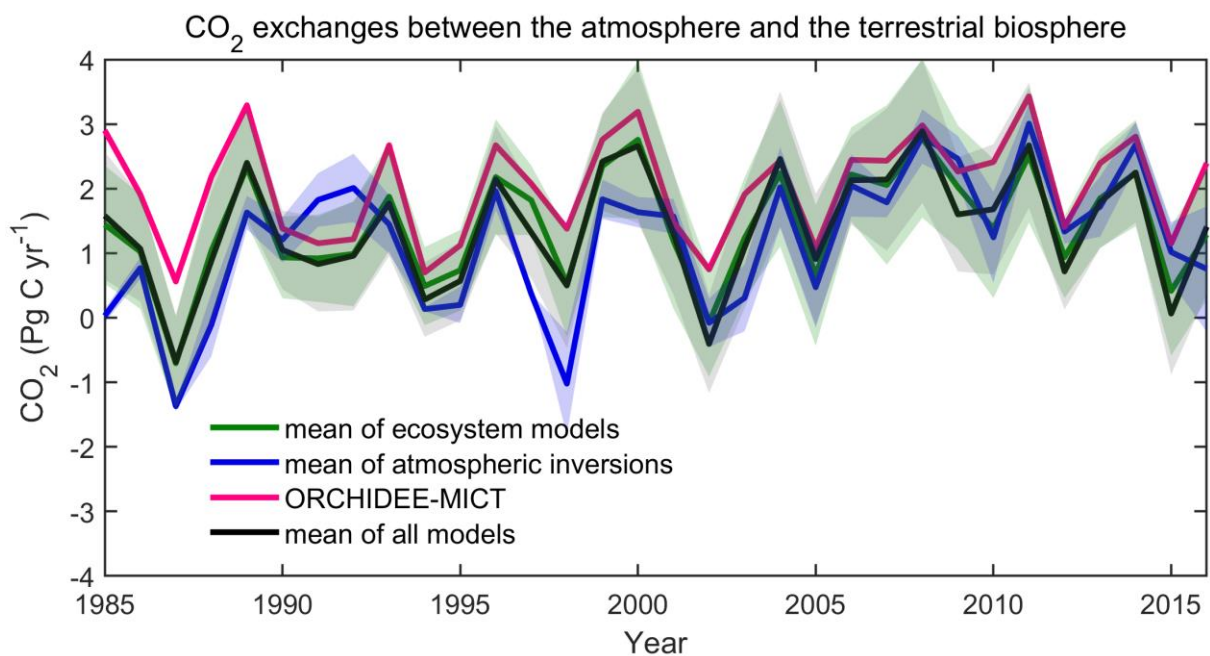


Figure S8

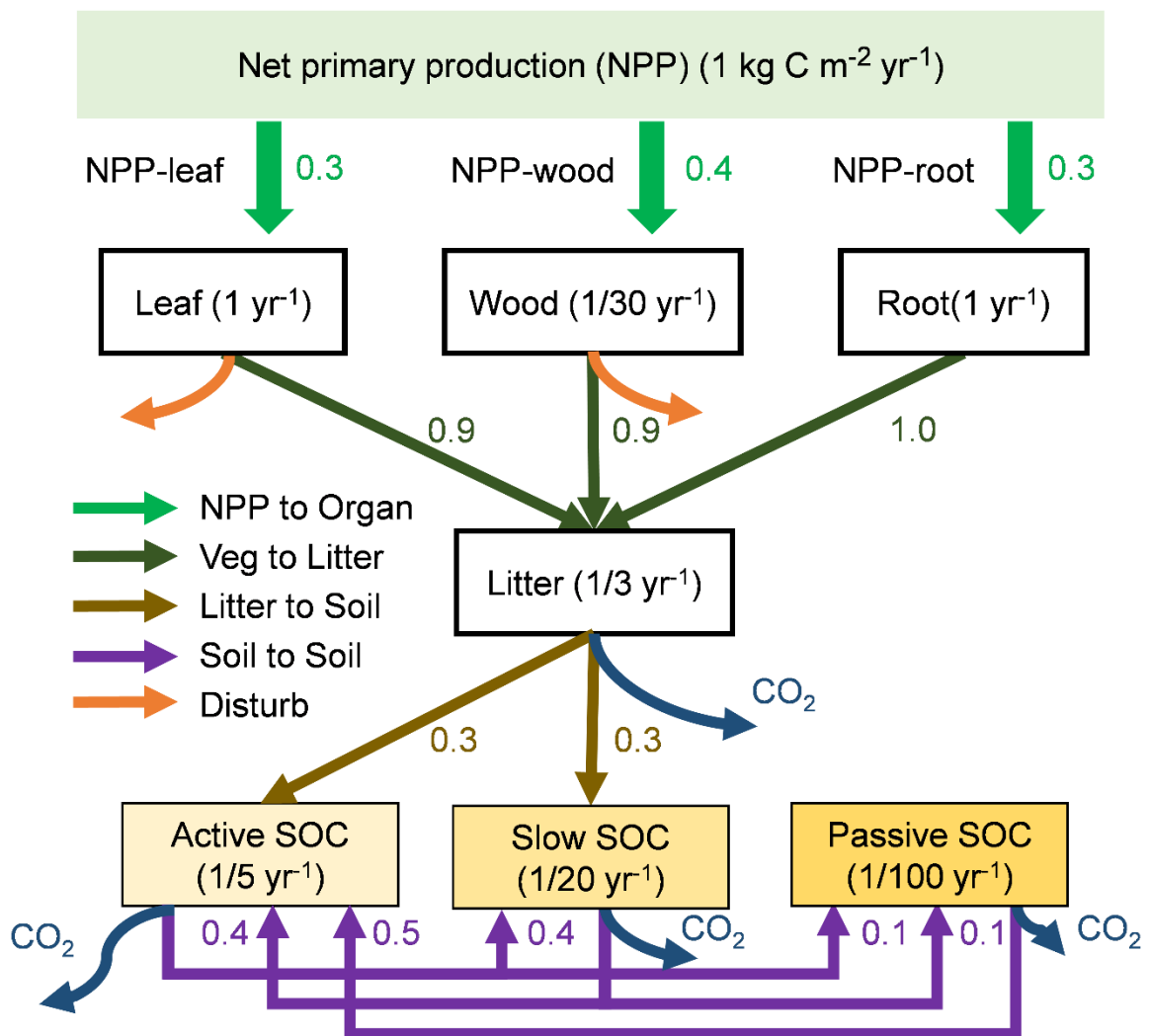


Figure S9

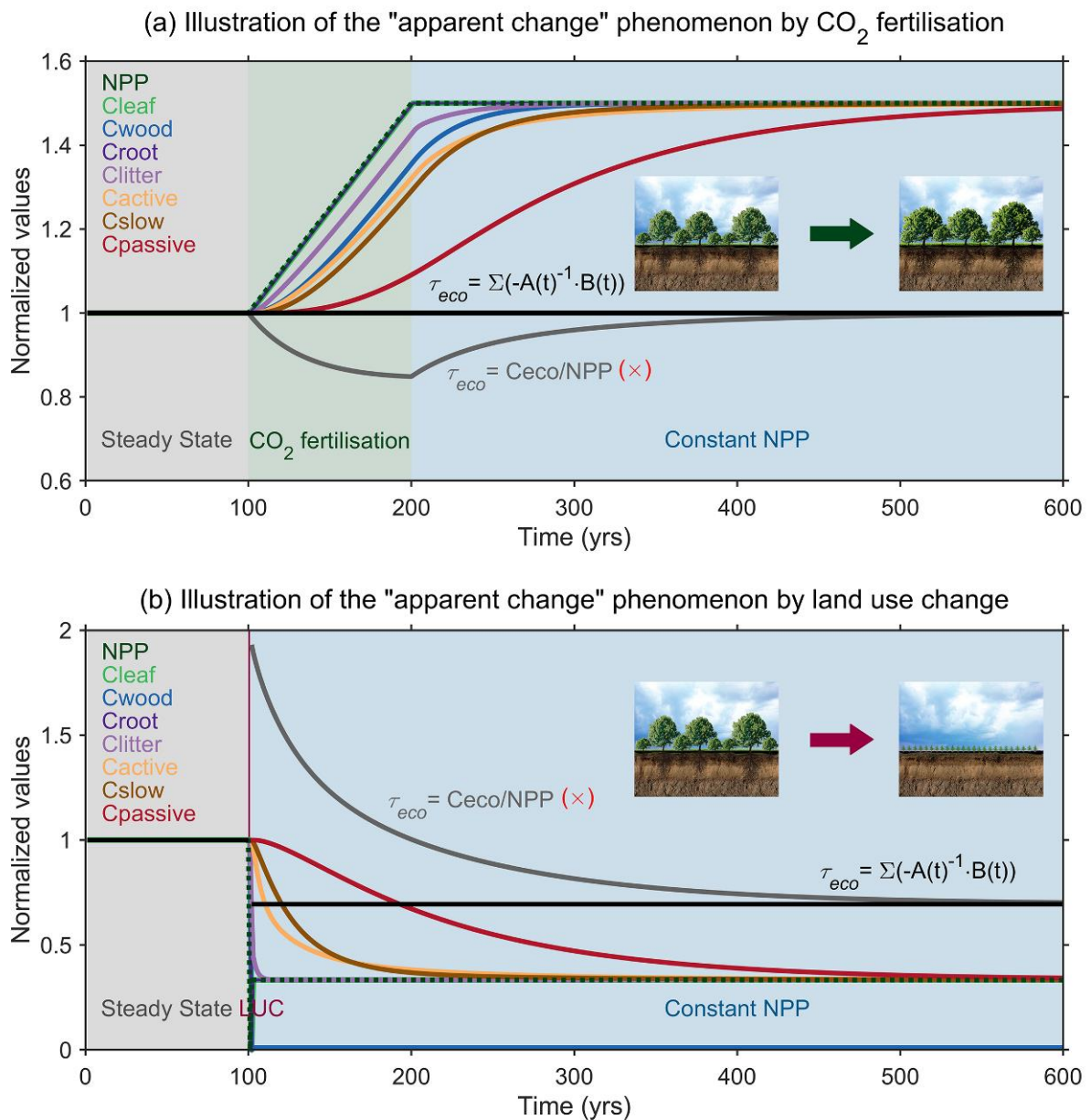


Figure S10

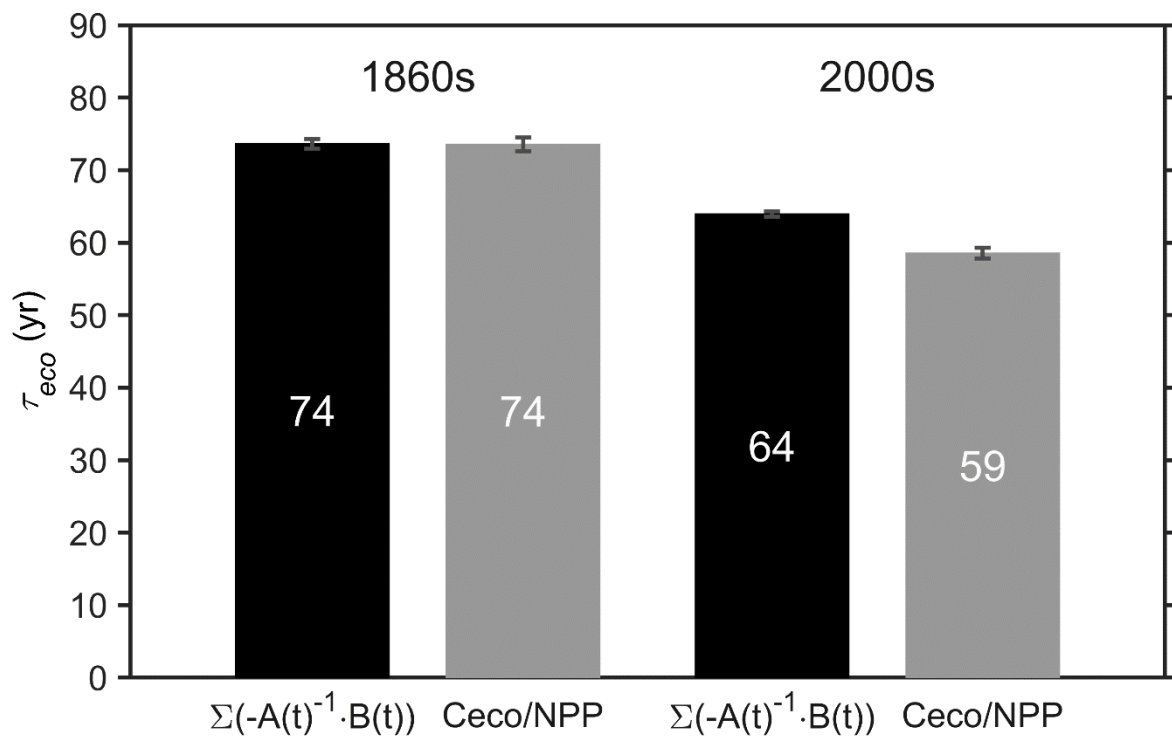


Figure S11

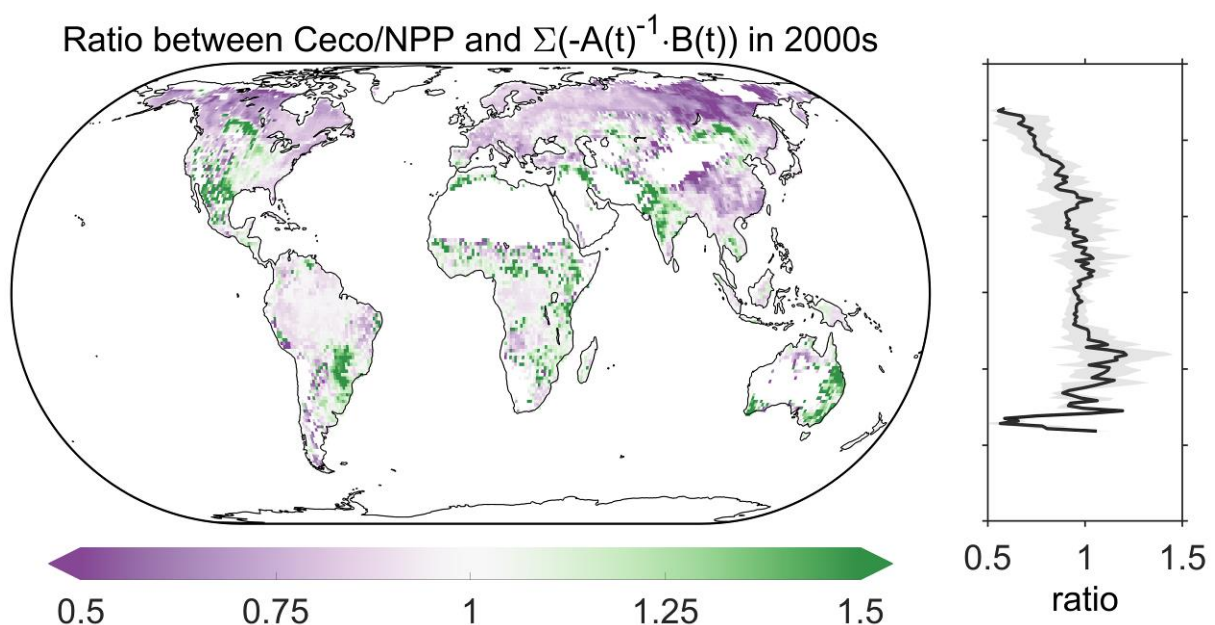


Figure S12

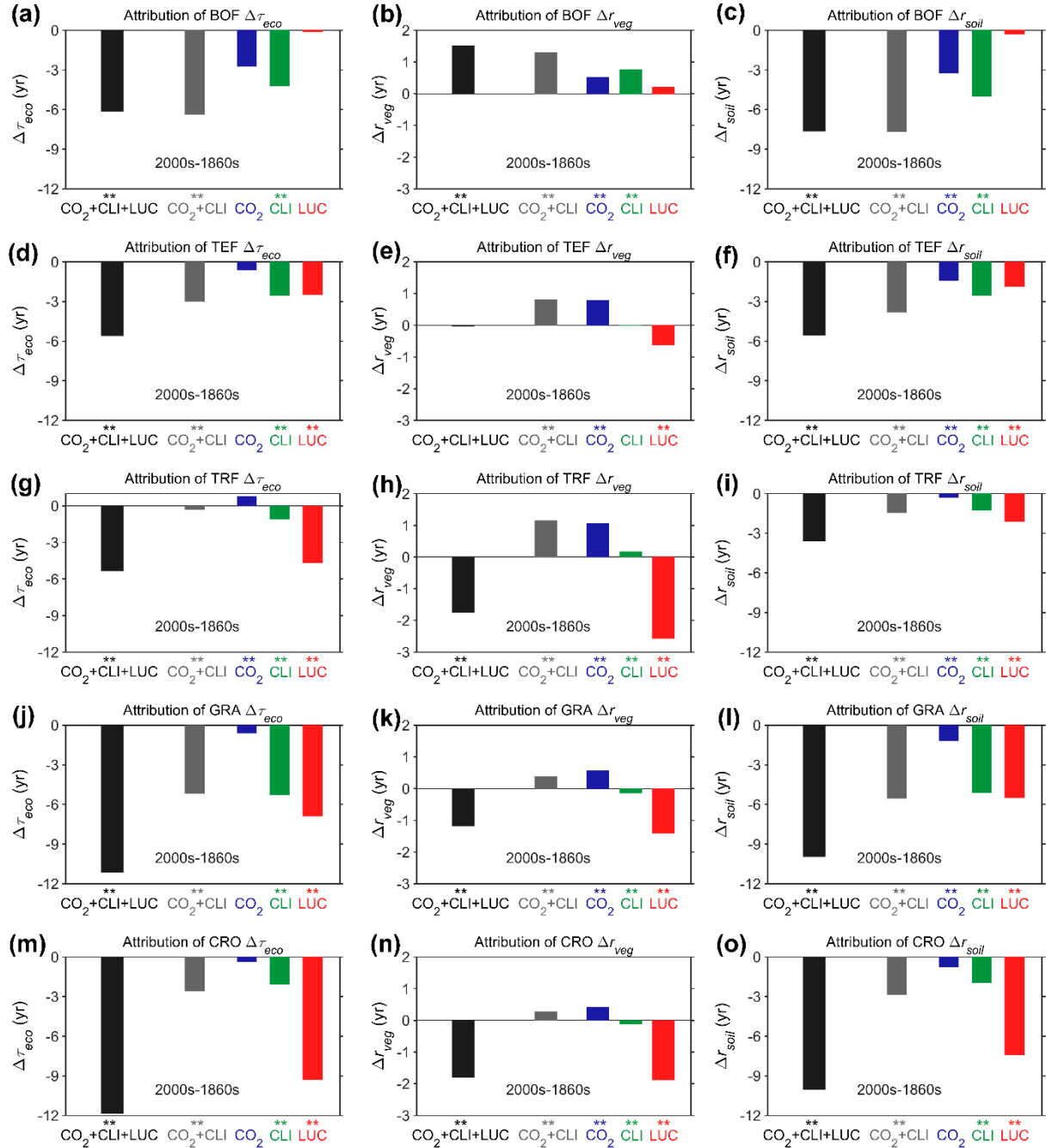


Figure S13

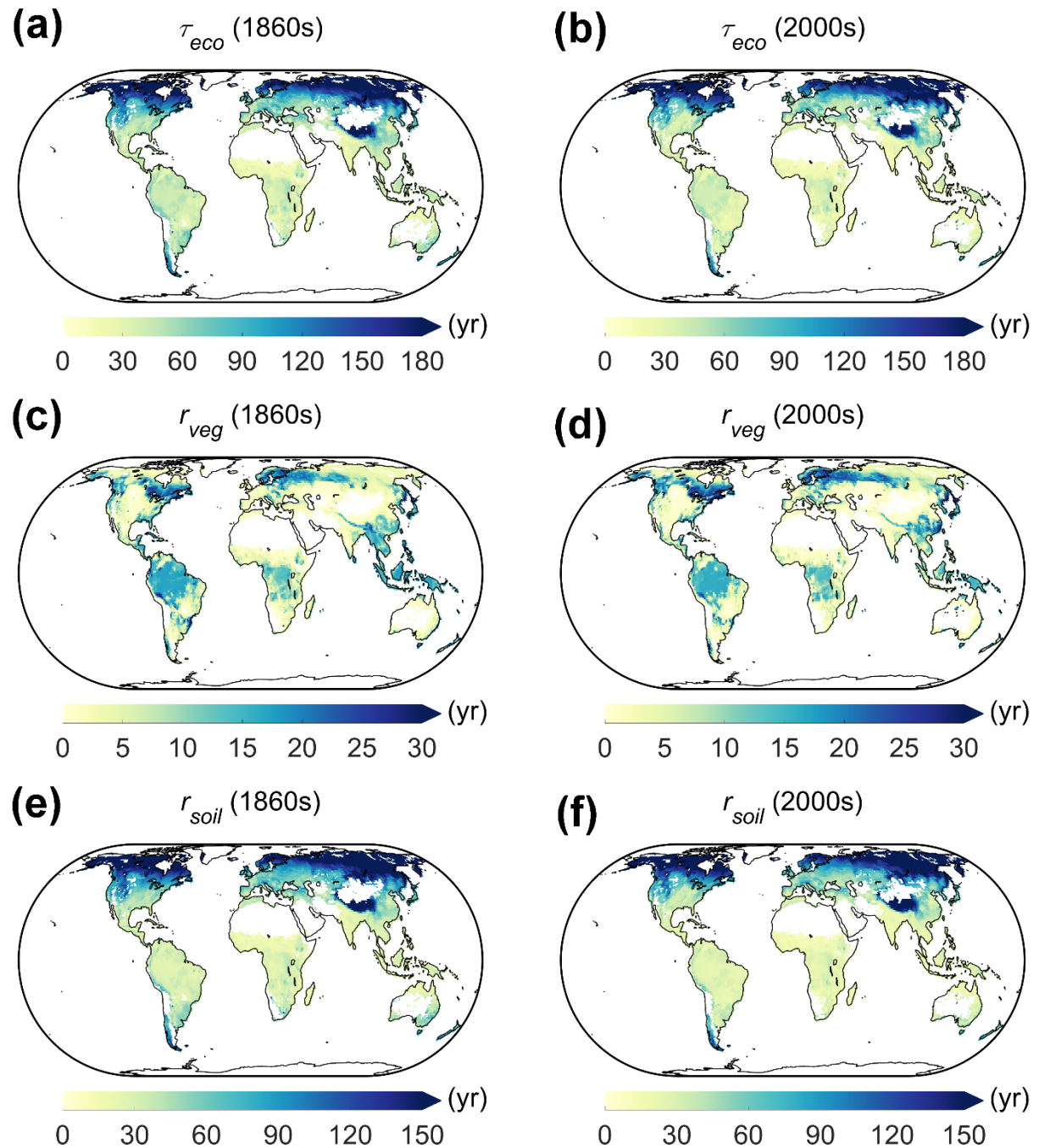


Figure S14

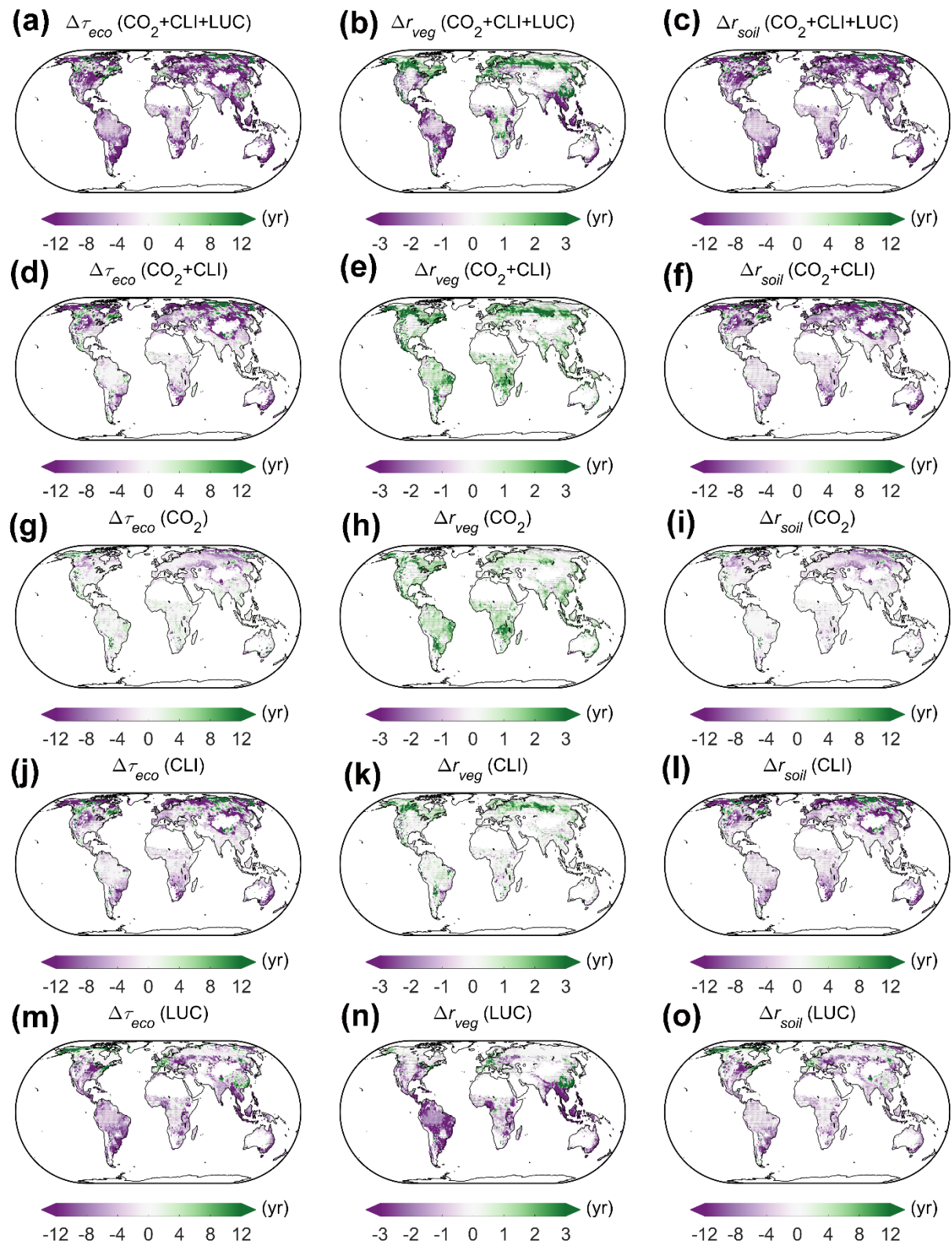


Figure S15

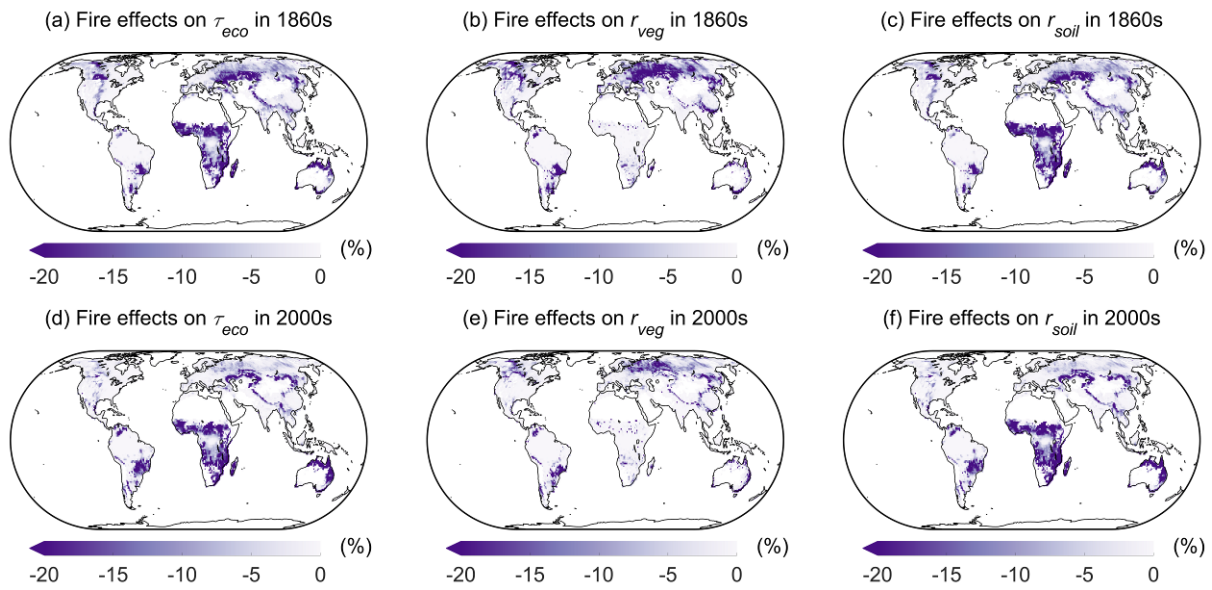


Figure S16

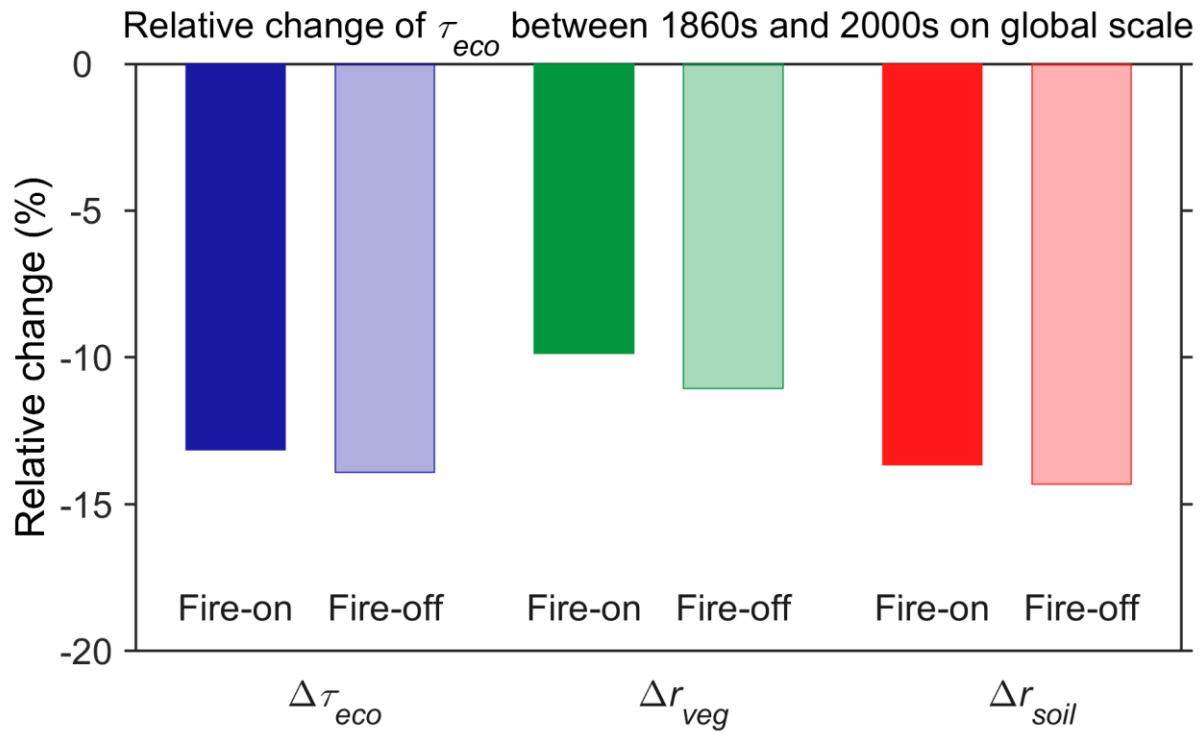


Figure S17

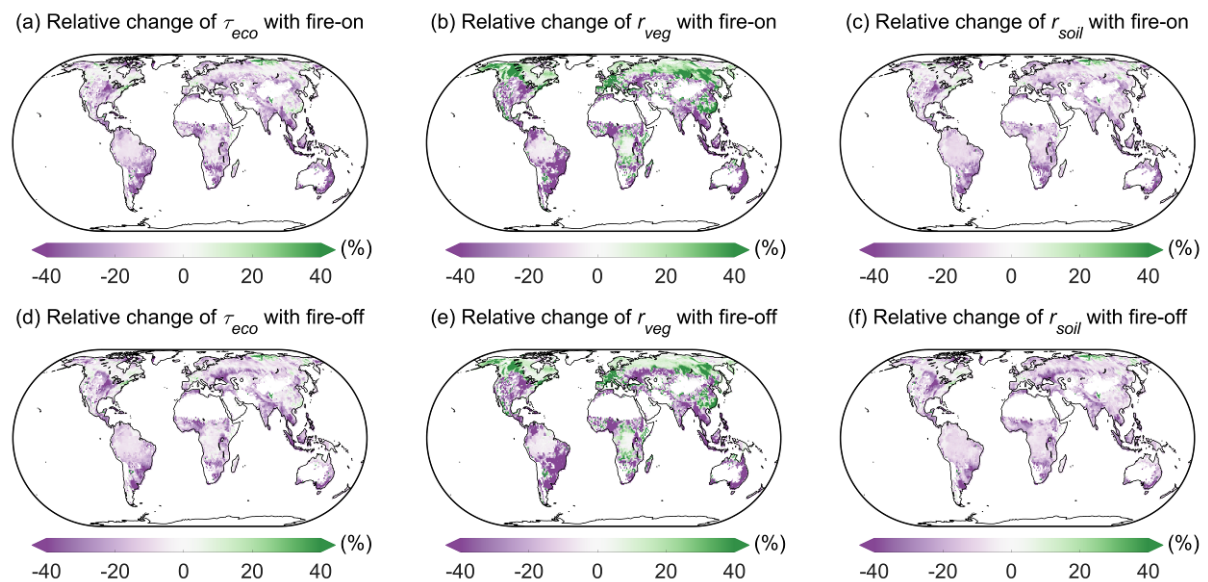


Figure S18

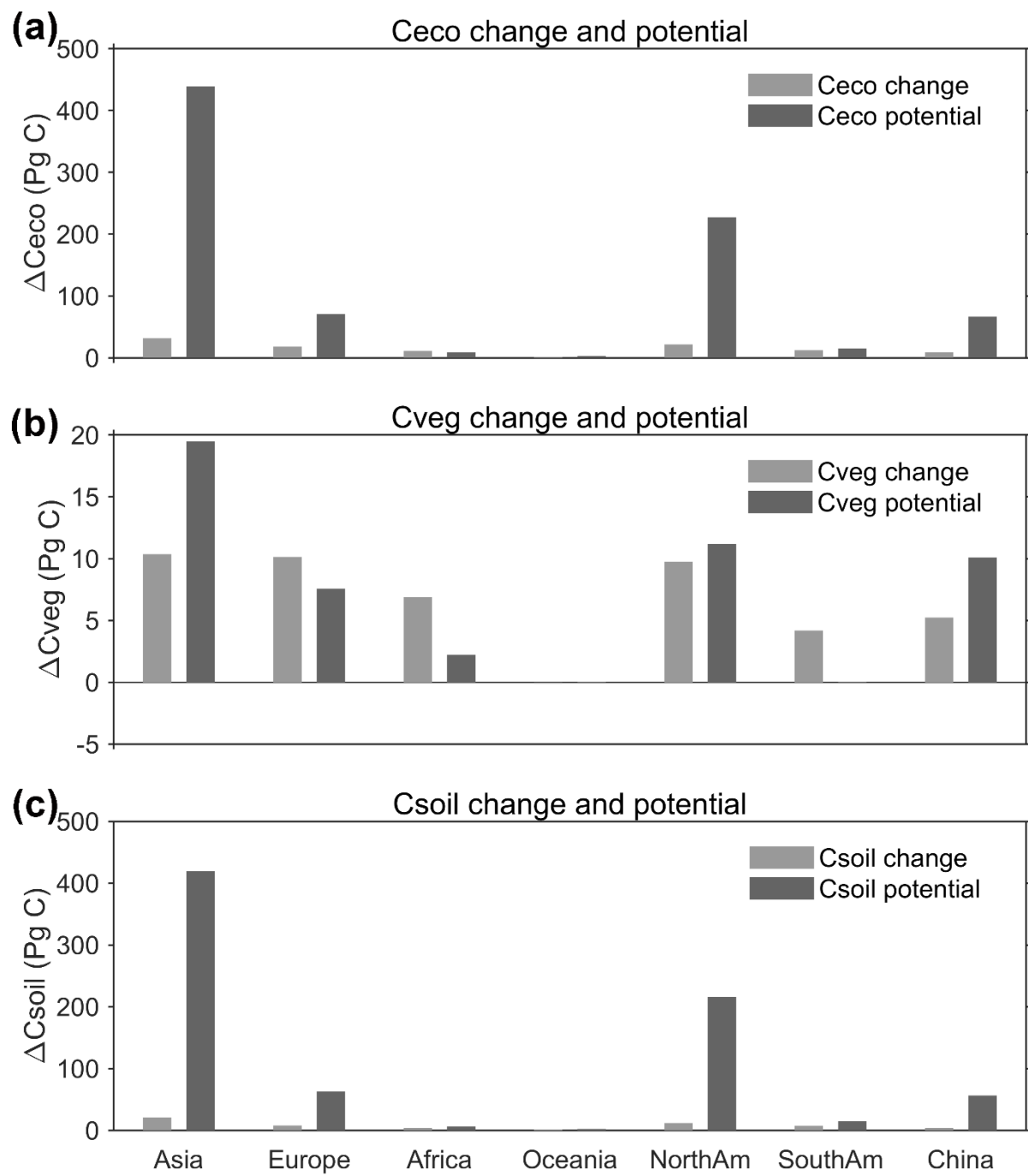


Figure S19

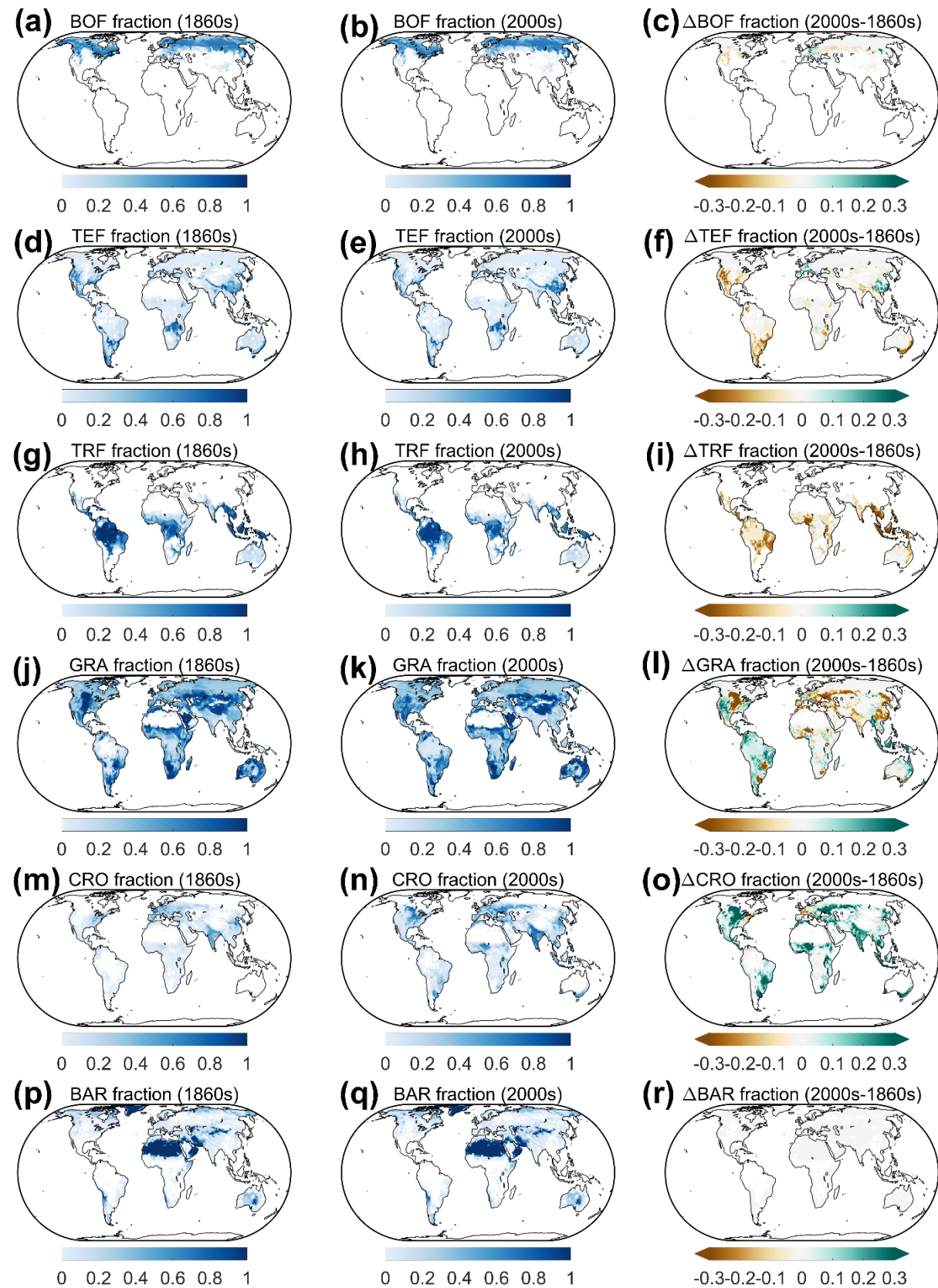


Figure S20

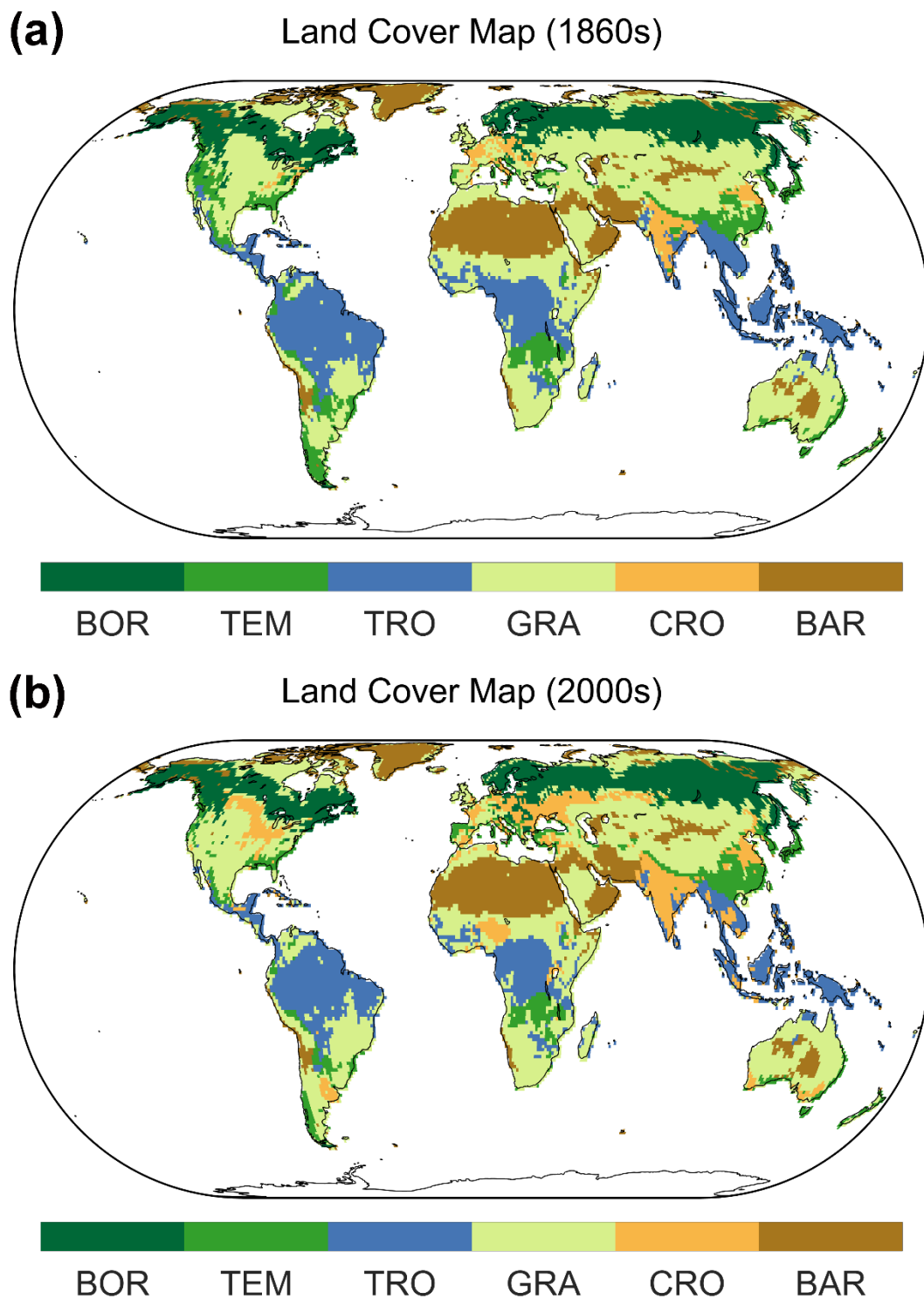


Figure S21

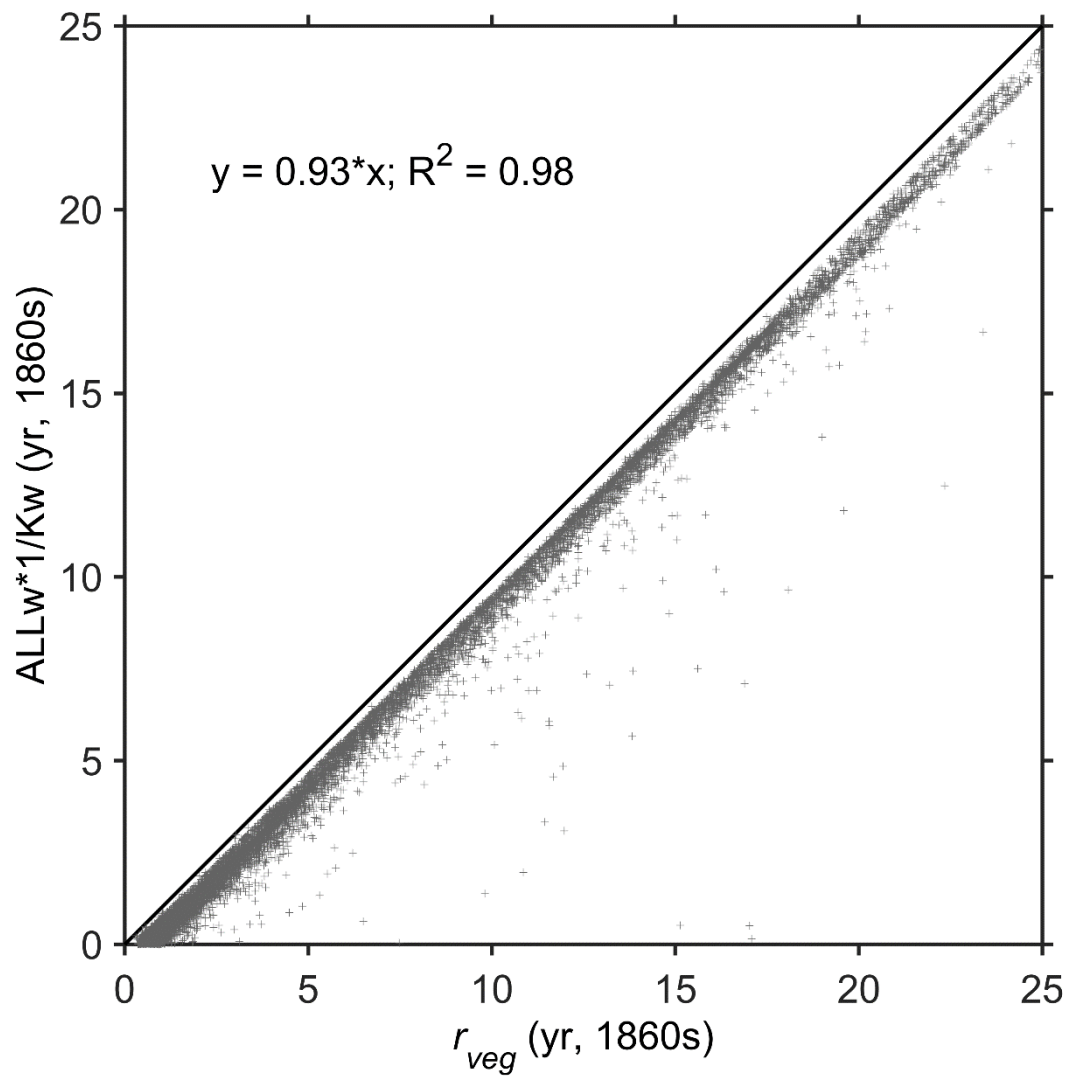
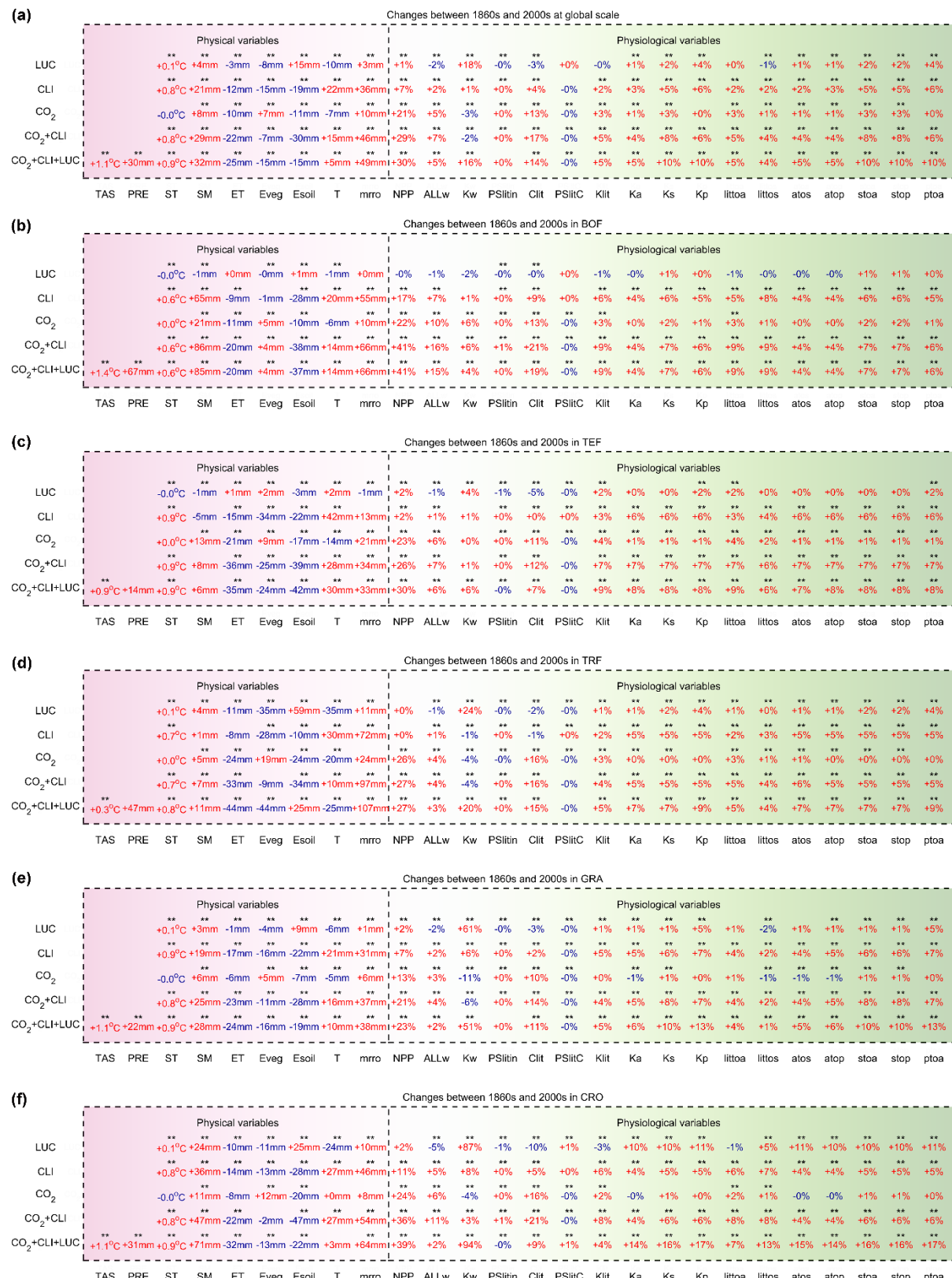


Figure S22



References:

- Bloom, A. A., Exbrayat, J.-F., van der Velde, I. R., Feng, L., & Williams, M. (2016). The decadal state of the terrestrial carbon cycle: Global retrievals of terrestrial carbon allocation, pools, and residence times. *Proceedings of the National Academy of Sciences*, 113, 1285-1290. <https://doi.org/10.1073/pnas.1515160113>
- Carvalhais, N., Forkel, M., Khomik, M., Bellarby, J., Jung, M., Migliavacca, M., . . . Thurner, M. (2014). Global covariation of carbon turnover times with climate in terrestrial ecosystems. *Nature*, 514(7521), 213-217. <https://doi.org/10.1038/nature13731>
- Guimberteau, M., Zhu, D., Maignan, F., Huang, Y., Yue, C., Dantec-Nédélec, S., . . . Laurent, P. (2018). ORCHIDEE-MICT (v8. 4.1), a land surface model for the high latitudes: model description and validation. *Geoscientific Model Development*, 11, 121-163. <https://doi.org/10.5194/gmd-11-121-2018>
- Hugelius, G., Bockheim, J. G., Camill, P., Elberling, B., Grosse, G., Harden, J. W., . . . Yu, Z. (2013). A new data set for estimating organic carbon storage to 3 m depth in soils of the northern circumpolar permafrost region. *Earth System Science Data*, 5(2), 393-402. <https://doi.org/10.5194/essd-5-393-2013>
- Jung, M., Reichstein, M., Schwalm, C. R., Huntingford, C., Sitch, S., Ahlström, A., . . . Zeng, N. (2017). Compensatory water effects link yearly global land CO₂ sink changes to temperature. *Nature*, 541(7638), 516-520. <https://doi.org/10.1038/nature20780>
- Kolby Smith, W., Reed, S. C., Cleveland, C. C., Ballantyne, A. P., Anderegg, W. R. L., Wieder, W. R., . . . Running, S. W. (2016). Large divergence of satellite and Earth system model estimates of global terrestrial CO₂ fertilization. *Nature Climate Change*, 6(3), 306-310.

<https://doi.org/10.1038/nclimate2879>

Le Quéré, C., Andrew, R. M., Friedlingstein, P., Sitch, S., Pongratz, J., Manning, A. C., . . . Zhu, D. (2018). Global Carbon Budget 2017. *Earth System Science Data*, 10(1), 405-448.

<https://doi.org/10.5194/essd-10-405-2018>

Liu, Y. Y., van Dijk, A. I. J. M., de Jeu, R. A. M., Canadell, J. G., McCabe, M. F., Evans, J. P., & Wang, G. (2015). Recent reversal in loss of global terrestrial biomass. *Nature Climate Change*, 5(5), 470-474. <https://doi.org/10.1038/nclimate2581>

Ruesch, A., & Gibbs, H. K. (2008). New IPCC Tier-1 global biomass carbon map for the year 2000. *Carbon Dioxide Information Analysis Center*, 1-7.

Thurner, M., Beer, C., Carvalhais, N., Forkel, M., Santoro, M., Tum, M., & Schmullius, C. (2016). Large-scale variation in boreal and temperate forest carbon turnover rate related to climate. *Geophysical Research Letters*, 43(9), 4576-4585.

<https://doi.org/10.1002/2016GL068794>

Thurner, M., Beer, C., Ciais, P., Friend, A. D., Ito, A., . . . Carvalhais, N. (2017). Evaluation of climate-related carbon turnover processes in global vegetation models for boreal and temperate forests. *Global Change Biology*, 23(8), 3076-3091.

<https://doi.org/10.1111/gcb.13660>

Wu, D., Piao, S., Liu, Y., Ciais, P., & Yao, Y. (2018). Evaluation of CMIP5 Earth System Models for the spatial patterns of biomass and soil carbon turnover times and their linkage with climate. *Journal of Climate*, 31, 5947-5960. <https://doi.org/10.1175/JCLI-D-17-0380.1>

Zhao, M., & Running, S. W. (2010). Drought-induced reduction in global terrestrial net primary production from 2000 through 2009. *Science*, 329(5994), 940-943.

<https://doi.org/10.1126/science.1192666>